Citation
Cui, L. and Zhang, X. and Hao, H. and Kong, Q. 2022. Improved resistance functions for RC elements accounting for compressive and tensile membrane actions. Engineering Structures. 251: Article No. 113549. http://doi.org/10.1016/j.engstruct.2021.113549

Improved Resistance Functions for RC Elements Accounting for Compressive and Tensile Membrane Actions

Liuliang Cui, Centre for Infrastructure Monitoring and Protection, School of Civil and Mechanical Engineering, Curtin University, Kent Street, Bentley, Australia, liuliang.cui@postgrad.curtin.edu.au

Xihong Zhang*, Centre for Infrastructure Monitoring and Protection, School of Civil and Mechanical Engineering, Curtin University, Kent Street, Bentley, Australia, xihong.zhang@curtin.edu.au.

Hong Hao, Centre for Infrastructure Monitoring and Protection, School of Civil and Mechanical Engineering, Curtin University, Kent Street, Bentley, Australia, hong.hao@curtin.edu.au.

Qingzhao Kong，College of Civil Engineering, Tongji University, 1239 Siping Road, Shanghai, P.R. China, qkong@tongji.edu.cn.

Abstract

Membrane actions commonly present in reinforced concrete elements as a result of restrained boundary conditions and geometry of deformations, which could substantially improve the ultimate flexural load-resistance as compared to that using yield line theory. Nevertheless, most current design manuals do not consider membrane effect because of a short of proper analysis method. This paper proposed an improved resistance model for RC (reinforced concrete) elements which considers both compressive and tensile membrane actions. Firstly, the derivation of the proposed membrane model was presented in detail. It was then validated with available testing data, in which good agreement was found on the load-deflection relationship of RC element between the estimation using the proposed model and testing data. Combining with the equivalent SDOF (single-degree-of-freedom) analysis method, the dynamic responses of structural

elements subjected to blast loads could be more accurately predicted as compared to the common elastic-perfectly-plastic resistance assumption in design guides. The proposed method was further verified with existing field blast testing results. Parametric studies were then carried out to examine the influences of critical design parameters for membrane behaviors including reinforcement ratio, span-to-depth ratio, and restraint stiffness. Last but not the least, based on the proposed analytical method a series of diagrams for modifying the design loading capacity estimated by UFC (Unified Facilities Criteria) design guides without considering the membrane effects were derived for more accurate and easy predictions of loading capacities in engineering applications.

Keywords: Membrane actions, RC element, resistance model, dynamic analysis, modification coefficient diagram.

1. Introduction

Terrorist bombing attacks and accidental explosion incidents impose substantial threatst to structure and personnel safety. For example, the recent accidental explosion in Beirut [1] caused at least 207 deaths, 7,500 injuries, and billions in property damage. Therfore, it is important to properly analyze and design structures against such extreme loading conditions. Abundent of experimental studies, numerial modellings, and theortical derivations have been performed over the past decades to study the resposnes of structures under extreme loading conditions [2-5]. Design standards such as UFC 3-340-02 [6] have also been developed to guide the analysis and design of civilian structures against blast loading. Previous studies found the ultimate flexural resistance capacity and response limit of structural elements such as reinforced concrete (RC) members with rigid boundary conditions can be much higher than those estimated following conventional design methods [7-9]. This is because the commonly used design standards employ yield line theory which

42 does not consider membrane forces when defining the resistance functions [10]. This underestimation in
43 structural resistance capacity could result in favourable “hiden” safety but in the meanwhile is uneconomical
44 for civilian structure design. Since during the service life of a civilan structure, the occurance of a blast event
45 is very low, the primary consideration of blast resistance design is collapse prevention and life safety.
46 Neglecting the memberane effect therefore leads to uneconomical designs of structures. Therefore, proper
47 undestanding and more accurate analysis and design is particularly necessary for civilian structures against
48 such extreme loading event.

49 Membrane forces predominately exist in RC elements as a result of element geometric deformation and
50 lateral restraint from the boundaries. Fig. 1 illustrates a typical load-deflection relationship for a restrained RC
51 element considering membrane effects. As described by Park and Gamble [11], when undergoing flexural
52 deformation, concrete cracks initiate at the bottom of the RC beam leading to a substantial shift in the position
53 of neutral axis, which causes the element edges tend to move outwards and react against the stiff bounday.
54 Therefore, an in-plain compressive membrane force is induced, and the ultimate flexural capacity of the
55 element is enhanced (segment OA in Fig. 1). As the deformation grows, concrete begins to crush and the
56 element will lose its flexural capacity until membrane forces in the central region change from compression to
57 tension (segment AB in Fig. 1). If the reinforcement is adequately anchored, tensile membrane forces will be
58 induced enabling the element to carry more loads. After point B, concrete cracks penetrate through the entire
59 depth of the cross-section, and the loads are mainly carried by reinforcement as a plastic tensile membrane.
60 Due to the presence of the tensile membrane action, the resistance of the RC element will increase with the
61 growth of element mid-span deflection until reinforcements fracture (segment BC in Fig. 1). The increase in
62 load resistance capacity accompanying this action is often called reserve capacity. A reserve capacity is

63 important in the design of protective structures since such structures are usually designed to sustain large
64 deflections and moderate to severe damage is often acceptable if collapse is avoided.

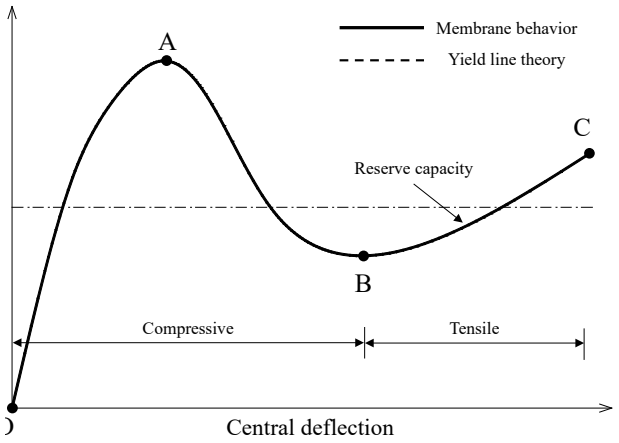

65
66 Fig. 1 Typical load-deflection relationship for restrained RC members considering membrane effects.

67 To understand the membrane effect, a number of experimental tests and theoretical studies have been
68 carried out by different researchers. Woodson [12] summarized experimental studies investigating the effects
69 of reinforcement details on the behavior of restrained RC members under transverse loading. It was concluded
70 with the support of previous testing data that design criteria for protective structures are overly conservative.
71 In addition, a total of 16 one-way restrained RC slabs was also performed under uniformly distributed static
72 pressure. It was found that the longitudinal reinforcement ratio has significant impacts on the ultimate flexural
73 bending capacity in the compressive membrane domain, as well as the reserve capacity in tensile membrane
74 domain. Park and Gamble [11] proposed a plastic theory for depicting the load-deflection behavior of a
75 restrained one-way RC slab in the compressive membrane domain. The yield line failure mechanism was
76 employed together with plastic hinges developed at critical sections to establish the geometric compatibility
77 condition of the RC element and the force equilibrium. However, the accuracy of Park and Gamble's
78 prediction method for the initial stiffness is in doubt because the plastic theory assumes that the plastic hinges
79 developed from the beginning of loading while in fact the element should be acting elastically or only partly

80 plastically at first. Besides, their method requires a predetermined mid-span deflection at the peak load
81 capacity to derive the resistance curve. To improve the drawbacks, Qian [13] and Chen et al. [14] identified
82 two phases in the compressive membrane domain based on material states, namely elastic phase and plastic
83 phase and adopted the flow theory to derive the load-deflection relationship. Before the yielding of tensile
84 reinforcements, concrete stress is calculated following Hooke's law, and is linearly distributed in the
85 compressive zone. After the yielding strain is reached, the compressive and tensile reinforcements are
86 assumed to yield simultaneously. Concrete will reach its ultimate compressive strength and behave perfectly
87 plastic. However, since concrete crushing and strength degradation is totally ignored, the resistance capacity
88 of the RC element in the plastic range is overestimated.

89 To depict the tensile membrane behavior of a RC element, Park [15] developed a theoretical model for
90 estimation of the load bearing capacity at large deflections. Later comparisons with testing results showed that
91 it is sometimes conservative if assuming only half of the reinforcements contribute to the tensile membrane
92 force but it overestimates the structural resistance when assuming all reinforcements would participate in the
93 tensile membrane force [12]. Meanwhile, the transition point from the compression membrane domain to the
94 tensile membrane domain would also affect the reserve capacity in tensile membrane domain, which therefore
95 needs to be determined as well [16, 17].

96 This paper aims to develop an improved analysis method incorporating membrane effect for RC element
97 against blasting loading. An improved resistance function considering both the compressive membrane effect
98 and the tensile membrane effect will be derived. Section 2 introduces the derivation of the model in detail,
99 which is verified through comparing the prediction of the resistance curves against existing testing results. To
100 further verify the effectiveness and accuracy of the proposed model in predicting the dynamic response of a

structural component against blast loading, the resistance functions of a series of RC beams derived with the proposed method is combined with the equivalent SDOF analysis. Comparisons are made between the analytical results and experimental data. Parametric studies are then carried out to examine the influences of different parameters on membrane actions. Last but not the least, a series of modification coefficient diagrams are generated based on the theoretical derivation which can be used to modify the resistance capacity estimated according to UFC-340-02 [6] approach without considering the membrane effect for more accurate predictions of the loading capacities of RC structures.

2. Derivation of Compressive and Tensile Membrane Models

Without losing generality, a RC beam is used herein for the derivation of the proposed compressive and tensile membrane model. The compressive membrane action and the tensile membrane action are described in detail below.

2.1. Theoretical model of compressive membrane behaviors

2.1.1. Membrane force-deflection relationship

The following assumptions are made during the derivation of the theoretical model for compressive membrane behaviors [14]: 1) Sections remain plane after flexural deformation; 2) Tension in concrete is neglected; 3) Shear deformation of the beam is neglected; 4) Beam deformation is assumed to concentrated at plastic hinges, and the segment between adjacent plastic hinges is straight; 5) Support rotation is assumed as fully restrained, thus surround rotational stiffness is considered as infinity.

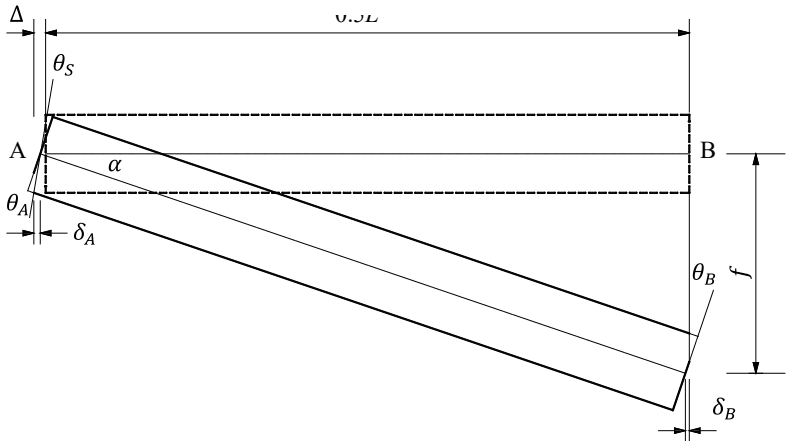

Fig. 2 Geometrical relationship of the deformed beam

The geometrical relationship of the deformed beam can be depicted as shown in Fig. 2, in which δ_A is the horizontal distance between the balanced point and midpoint of section A; δ_B is the horizontal distance between the balanced point and midpoint of section B; Δ is the horizontal movement of support; θ_s represents support rotation; θ_A and θ_B represent the rotation of section A and B. By referring to Qian's method [13], the compressive membrane force-deflection relationship can be expressed as

$$\frac{dN}{df}=\frac{(\eta_A+\eta_B)h\dfrac{1}{0.5L}-\eta_A h\dfrac{4}{LL_p\dfrac{S_m}{EI}+L}-f\dfrac{1}{0.5L}}{\dfrac{1}{S_n}+\dfrac{0.5L}{E_c bh+E_s(A_s+A_{ss})}} \tag{1}$$

The derivation details can refer to ref [13]. Since support rotation is assumed to be fully restrained, support rotational stiffness S_m is considered as infinity, Eq. (1) would turn into

$$\frac{dN}{df}=\frac{(\eta_A+\eta_B)h\dfrac{1}{0.5L}-f\dfrac{1}{0.5L}}{\dfrac{1}{S_n}+\dfrac{0.5L}{E_c bh+E_s(A_s+A_{ss})}} \tag{2}$$

in which

$$\eta_A h=0.5h-x_n^A \quad \text{and} \quad \eta_B h=0.5h-x_n^B \tag{3}$$

where N represents the compressive membrane force induced by the lateral movement of the supports; f is the mid-span deflection of the beam; S_n is the lateral stiffness of support, which will be always compared

with the elements' axial stiffness S_a that can be calculated by $S_a = 2bhE_a / L$, $E_a = [E_c(h - 2\rho h_0) + 2E_s \rho h_0)]/h$ [14]; ρ is the reinforcement ratio; E_c and E_s are the elastic modulus of concrete and reinforcement; x_n^A and x_n^B are the depths of the neutral axis (depth of compressive zone) of cross section A and B; A_s and A_{ss} are the area of reinforcement in tension and compression; L, h, b are the length, depth and width of the beam; I_a is the averaged moment of inertia of the beam which can be calculated following UFC 3-340-2 [6]. Therefore, the membrane force *N* can be obtained by solving this integration equation.

2.1.2. Deformation and force relationships of the cross section

The main difference between the resistance functions of a restrained RC beam and a simply supported beam is the consideration of axial force. Given the membrane force derived from section 2.1.1, the membrane-dependent moment-curvature relationship can be obtained through layered analysis of cross-section. Fig. 3 shows the layered cross section of a doubly reinforced RC element and its stress and strain diagram. The stress and strain within each layer are assumed to be constant. Neglecting the tensile strength of concrete, the following force equilibrium equation of cross section must be fulfilled at each instant:

$$N + \sigma_s A_s - \sigma_{ss} A_{ss} - \sum_{i=1}^{i=n} \sigma_{ci} A_{ci} = 0 \tag{4}$$

where σ_s and σ_{ss} are the stresses in the tensile and compressive reinforcements; n is the number of concrete layers in compression; σ_{ci} is the compressive stress of the *i* th layer of concrete; A_{ci} is the area of the *i* th layer of concrete, and $A_{ci} = bx_n / n$, of which b is the width of cross section and x_n is the depth of neutral axis. Taking moment equilibrium about the neutral axis, the resultant moment M_R can be calculated by

$$M_R = \sigma_{ss} A_{ss} (\frac{h}{2} - d_c) + \sigma_s A_s (h_0 - \frac{h}{2}) + \sum_{i=1}^{i=n} \sigma_{ci} A_{ci} y_{ci} \tag{5}$$

where d_c is the depth of the concrete cover; h_0 is the effective depth; and y_{ci} is the distance from the *i* th

layer of concrete to the neutral axis. The corresponding curvature φ is computed by

$$\varphi = \frac{\varepsilon_s}{h_0 - x_n} \tag{6}$$

where ε_s is the strain in the tensile reinforcement. Based on equations (4), (5) and (6) the moment-curvature relationship of the critical sections considering compressive membrane forces can be obtained.

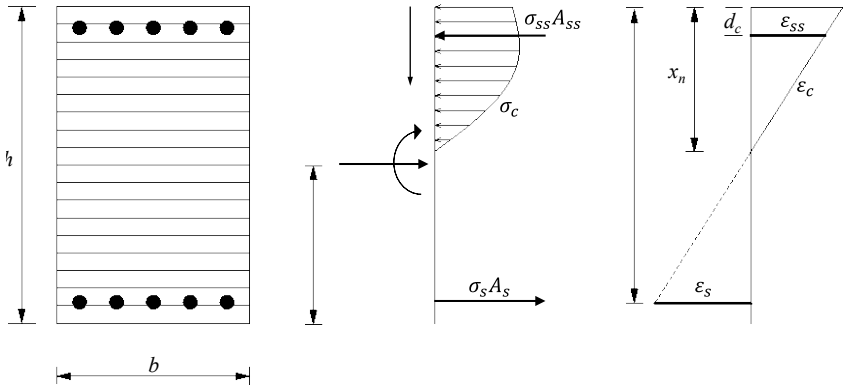

Fig. 3 (a) Layered cross section of a doubly reinforced RC element; (b) stress diagram of cross section; (c) strain diagram of cross section

The constitutive properties of concrete adopt the idealized stress-strain curve for concrete under uniaxial compression as proposed by Hognestad [18]. The ascending branch of the stress-strain relationship, when $0 \le \varepsilon_c \le \varepsilon_m$, is described by the following equation:

$$\sigma_c = f_{cm}\left[\frac{2\varepsilon_c}{\varepsilon_m} - \left(\frac{\varepsilon_c}{\varepsilon_m}\right)^2\right] \tag{7}$$

The descending branch, where $\varepsilon_c > \varepsilon_m$, is a straight line connecting the peak strength f_{cm} to $0.85f_{cm}$ at a strain of ε_u. To account for the degradation of concrete strength, the slope of the descending branch remains constant until stress drops to $0.2f_{cm}$ at a strain of ε_{lim}. Generally, $\varepsilon_m = 0.002$ and $\varepsilon_u = 0.0038$. The uniaxial behavior of reinforcing steel (both in tension and in compression) is approximated to be elastic-perfectly-plastic.

It is worth noting that preliminary calculation of the section moment-curvature relationship shows that as

the maximum concrete compressive strain approaching ε_{lim}, the resistance capacity exhibits a clear decreasing tendency. However, beyond ε_{lim} the numerical calculation may cease because the stress in concrete is too small to achieve force equilibrium at the cross section when membrane force is large. This contradicts with experimental observations that a RC element will usually not rupture suddenly but continues to deform due to stress redistribution. For structural elements under blast loading, the whole resistance-deflection curve is an essential prerequisite for predicting the dynamic responses. Therefore, to construct a complete resistance function accounting for softening effect resulted from concrete crushing and spalling as well as to improve the computational efficiency, the moment-curvature relationship is modified as shown in Fig. 4 (a) and (b). When the maximum concrete compressive strain reaches ε_{lim}, the original computation model stops automatically. In the modified model, the moment descending is further extended, following the same slop of line AB until moment capacity drops down to 0.1 M_{max}, and then the moment capacity maintains at this level as the residual strength. This modification helps to ensure computational stability while best replicates the ductile behavior of a flexural deformed RC element.

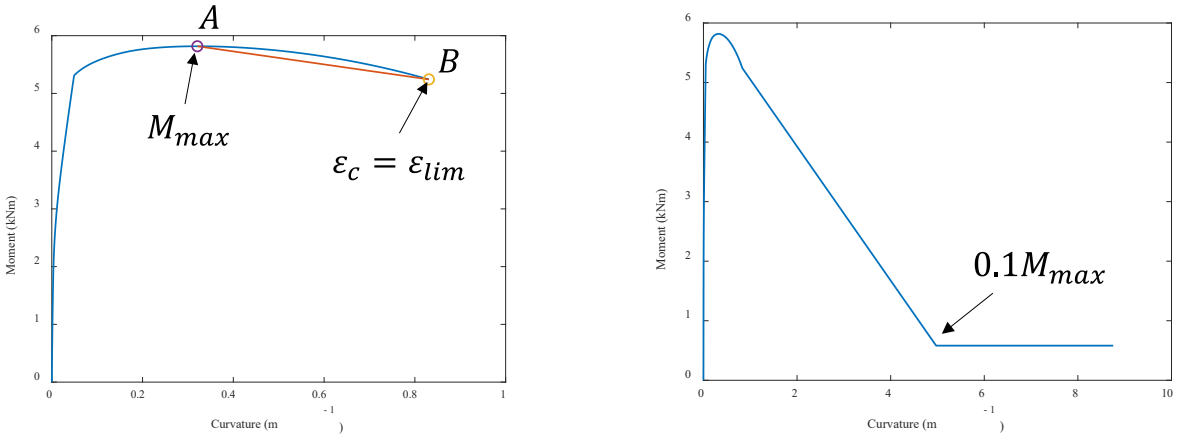

(a) (b)

Fig. 4 (a) Original moment-curvature relationship, and (b) modified moment-curvature relationship.

2.1.3. Determination of resistance function

As pointed out above that Park's theory [11] cannot accurately predict the initial elastic behavior of a RC element because of the plastic hinge assumption as described in Section 2.1.1. The theoretical model assumes that the deformation concentrates at the plastic hinges located at support and midspan while the segments between two plastic hinges remain straight. This assumption may be reasonable after the yielding of reinforcement, but not for the initial elastic response of the RC element where the deformation of a beam should be a smooth curve. This simplification overestimates the initial stiffness of the resistance curve and causes the curvature at critical sections change abruptly. To overcome this shortage, in the proposed model, the curvature-deflection relationship in the elastic range follows the actual deformation shape (elastic deformation shape). Before the yielding of bottom reinforcement, it is considered that the RC beam behaves elastically. For simplicity, it is assumed that the curvature changes are the same at supports and mid-span for the same deflection increment. Therefore, the curvature-deflection relationship at support and mid-span can be obtained following the fundamental theory of mechanics of materials as

$$d\varphi = \frac{LK_E}{8E_cI_a}df \tag{8}$$

in which K_E is the elastic stiffness of the resistance function of the beam. Since there is no significant deformation in elastic range and membrane effect is negligible, the stiffness in elastic range K_E can be taken as the same value as that for a simply supported beam. Therefore, K_E can be calculated by [19]

$$K_E = \frac{384E_cI_a}{5L^4} \tag{9}$$

E_c is the modulus of elasticity of concrete, and I_a is the average moment of inertia of the beam.

After the tensile reinforcements yield, plastic hinges are developed. The curvature-deflection relationship changes into,

$$d\varphi = \frac{4df}{LL_p} \tag{10}$$

where L_p is the plastic hinge length, which can be calculated by the simple formula used by Fujikake [20] as

$$L_p = h_0 + 0.05L \tag{11}$$

Eventually, the resistance capacity of the element can be obtained based on static equilibrium equations. For a restrained beam under uniformly distributed load, the resistance q can be computed by

$$q = \frac{8}{L^2}(M_R^A + M_R^B - Nf) \tag{12}$$

where q is the external load (force per unit length), M_R^A and M_R^B are the resistant moments at support (section A) and midspan (section B).

2.2. Theoretical model of tensile membrane behaviors

As illustrated in Fig. 1, after reaching the ultimate flexural load resistance capacity (point A in Fig. 1), the load resistance capacity of the beam will decrease rapidly with further imposed deflection because of concrete crushing and the reduction in the compressive membrane forces [11]. If the reinforcement of the RC beam is adequately anchored into adjacent supports, tensile membrane behavior could be developed. As depicted in Fig. 1 for point B, the membrane forces in the central region of the beam change from compression to tension and the beam boundary restraints begin to resist inward movement of the edges.

To analytically derive the tensile membrane force, it is assumed that: (a) concrete cracks throughout the entire depth of the beam, and hence is incapable of carrying any load; (b) all the reinforcement reaches the yield strength and hence acts as a plastic membrane; (3) no strain hardening of steel occurs; and (4) only the reinforcement that extends over the entire area of the RC beam contributes to the membrane action. Based on Park and Gamble's theory [11], the tensile membrane resistance (uniform load per unit area), q_T, of a

laterally restrained element at a midspan deflection, f_m, can be expressed as:

$$q_T = 8T_y f_m / L^2 \tag{13}$$

where T_y is the yield force of the reinforcement per unit width; and L is the clear span length. Using Equation (12), the slope of the tensile membrane effect in the resistance-deflection curve can be determined. It is worth noting that the amount of principal reinforcements that contribute to tensile-membrane action depends on the reinforcement details and end anchorage. While in theoretical models, two typical cases are usually assumed: 1) all principal reinforcements in each face contribute to tensile-membrane action, or 2) only half of the principal reinforcements (tensile reinforcement) contribute to tensile-membrane action.

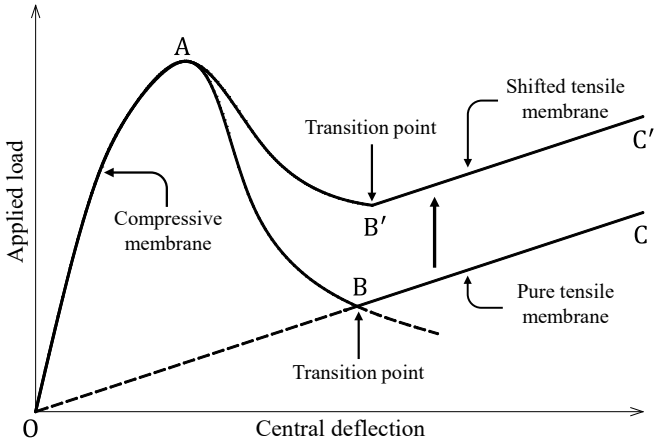

Fig. 5 Combined compressive-tensile membrane resistance model.

To construct a complete and continuous compressive-tensile membrane resistance model, the load-deflection curves obtained in compressive and tensile membrane domains need to be combined, as shown in Fig. 5. As noted earlier, the transition point B usually represents the instant that the membrane forces changing from compression to tension. However, in the compressive membrane model, the point where the membrane force turning into zero does not always fall on the pure tensile membrane line. Therefore, two possible scenarios exist: if the descending branch of the compressive membrane curve (*AB*) intersects with the tensile membrane line (*OC*), the intersection point would be the transition point, and after that point, resistance would

switch from the compressive membrane mode to the tensile membrane mode (*OABC* in Fig. 5). If they do not intersect, the original tensile membrane line (*OC*) could be shifted upwards slightly to connect with the lowest point of the descending branch of the compressive membrane curve so as to form the resistance curve $OAB'C'$, as recommended by Krauthammer [10, 17]. Therefore, a complete load-deflection relationship covering both the compressive and tensile membrane effects can be constructed.

3. Model Validation

To examine the suitability and accuracy of the proposed model considering both the compressive and tensile membrane effects, in this section the proposed modeling method is used to predict and compare with existing testing data available in the literature.

3.1. Static resistance function

3.1.1. Experimental information

Woodson carried out a series of laboratory tests on one-way RC slabs to study membrane action [12]. The slabs were clamped with steel plates to restrain their transverse and rotational movements. Water pressures were used to uniformly load the slabs to obtain their static resistance functions. Each slab had a clear span of 609.6mm (24 inch), a width of 609.6mm (24 inch), and an overall depth of 76.2mm (3 inch). The effective depth of slabs was 609.6mm (2.4 inch). All slabs were equally reinforced. In this paper, the tested slab No.4 and No.9 were chosen for analysis with reinforcement ratios of 0.25% and 0.97%, respectively. These two slabs had the same concrete strength of 30 MPa but different reinforcement yielding strength of 414 MPa and 500 MPa for slab No. 4 and No. 9, respectively. It is worth pointing out that according to Woodson [12] the supports were fully restrained against rotational and vertical translation but partially restrained against lateral

displacement as compressive membrane action is dependent on the lateral restraint. In the following analysis, the lateral stiffness of support is taken as $1.41\times10^{8} N/m$ which is about 0.023 times the axial stiffness of the slab element. This value is determined by try and error through the theoretical model since the actual value is not provided in the test because it is difficult to measure.

3.1.2. Comparison of the resistance functions

Following the proposed method as detailed in Section 2, considering both the compressive and tensile membrane effects, the load-deflection curves of slab No.4 and No. 9 can be derived (as shown in Fig. 6). For better comparison, compressive and tensile membrane models are plotted separately, i.e. C-M (Cui) for the compressive membrane domain and T-M (Half steel) and T-M (Total steel) for the tensile membrane domain considering only tensile reinforcement and both compressive and tensile reinforcements. To compare the effectiveness of the proposed method, the predictions from the commonly used design standard UFC 3-340-02 is also included. According to UFC, the ultimate resistance of a fully fixed beam is calculated by

$$R_{UFC} = \frac{8}{L^2}(M_u^s + M_u^m) \tag{14}$$

where M_u^s and M_u^m represent the ultimate moment capacity at beam end and midspan. When the longitudinal reinforcement is extended into supports and assuming the tension and compression reinforcements are equal,

$$M_u^s = M_u^m = A_s f_y d \tag{15}$$

where d is the distance between the centroids of the compressive and tensile reinforcement. Besides, existing theoretical derivation formula for membrane effect by Chen et al. [14] is also compared herein.

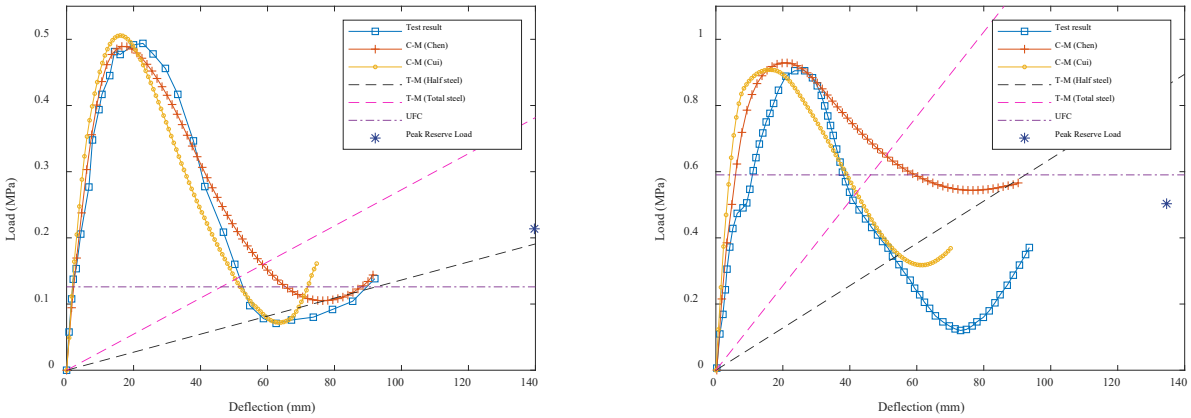

(a) Slab No. 4 (b) Slab No.9

Fig. 6 Comparison of different resistance functions of (a) slab No. 4 and (b) slab No. 9

As can be seen in Fig. 6, in the compressive membrane domain the resistance curves derived using the proposed model in this study are quite close to the testing results for both Slab No. 4 and No. 9. Comparing with Chen et al.'s model, the descending behaviors of the proposed model agree much better with the test results. This improvement is attributed to the consideration of concrete softening behavior and the modification of moment-curvature relationship.

As the mid-span deflection further increases, the resistance load gradually increases after the descending stage. However, because of the inaccurate measurements of the deflection gage at large deflections, Woodson did not provide the complete resistance-deflection curves for the reserve capacity (i.e. the tensile membrane region). Instead, the ultimate reserve capacities and the ultimate deflections measured post the tests were provided. As can be observed in Fig. 6 (a), for slab No.4 the peak reserve load is higher than the prediction of UFC. The prediction using the proposed method considering only the tensile reinforcement agrees well with the testing data. Nevertheless, for slab No. 9 the lab measured peak reserve capacity is far less than the prediction of the proposed method, which is also smaller than those of the UFC methods that do not take account of membrane effect, reflecting the measured reserved load is very small. This was explained by Woodson that there existed pull-out or slip of reinforcements because of insufficient anchorage. In view of

this, for engineering practice, it is more reasonable and conservative to assume that only half of the reinforcement is contributing to tensile membrane action, because it is unsure whether all the reinforcements would have been anchored properly; even so, steel rupture cannot be avoided at large deflection.

3.2. Dynamic analysis using the proposed model

To examine the suitability and accuracy of the proposed method for predicting structural response under severe dynamic loading (impact or blast loads), the proposed model is utilized to perform dynamic structural analysis based on a single-degree-of-freedom (SDOF) approach. The general method of converting a structural component into an equivalent SDOF system was discussed in details by Biggs [19]. Previous testing results by Keenan [7] is used for comparison and model verification.

3.2.1. Test information

In Keenan's test program, four one-way RC slabs were subjected to uniformly distributed loads: slab S1 was subjected to an increasing static load (water pressure) until failure to determine its static load-deflection curve; the other three (D1, D2, D3) were subjected to explosive loads to analyze their dynamic behaviors. All slabs were fully clamped restraining their longitudinal, transversal and rotational degrees of movement. The clear span, the width and the depth of those slabs were 1828.8 mm (6 feet), 609.6 mm (24 inch) and 152.4 mm (6 inch), respectively. The cross section was symmetrically reinforced with 2.11% of tensile reinforcement. The concrete compressive strength was 37.4 MPa and the yielding strength of the reinforcement was 344MPa. More details about the test can be found in reference [7].

3.2.2. Comparison of the static load-deflection curve of slab S1

Since both the ends of the slab were fully restrained against rotation, and partially but strongly restrained against the longitudinal movement, in the theoretical analysis in this study, the rotational stiffness of the support is considered as infinity and the lateral stiffness is assumed the same as the axial stiffness of half slab ($6.1\times10^{9} N/m$). Fig. 7 shows the comparison of different static resistance models of slab S1, in which red solid curve is the derived compressive-tensile membrane model using the proposed method in this paper. Noting that in the tensile membrane domain, only the tensile reinforcement is assumed to contribute to the tensile membrane action. It was reported by Keenan that at a mid-span deflection of 147 mm, a wedge of concrete about 127 mm long was sheared loose from a loaded edge of the slab near the mid-span. This local failure destroyed the water seal and prevented the further increase of slab deflections. Therefore, the tensile membrane behavior was not recorded in the test.

For comparison, the resistance function derived using design standard UFC 3-340-02 which does not consider membrane effect is also include in Fig. 7. Following the UFC code, an elastic-perfectly-plastic resistance function is considered.

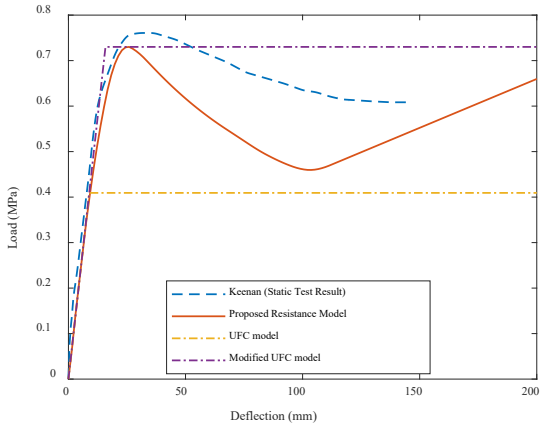

Fig. 7 Comparison of different static resistance models of slab S1

It can be seen from Fig. 7 that compared to the resistance function suggested by UFC, the proposed

theoretical resistance model considering membrane effect agrees much better with the testing result. The measured resistance load is slightly larger than the theoretical prediction because of friction between the vertical side of the slab and the vertical wall of the loading box (according to Keenan). It is apparent that the prediction using the UFC method greatly underestimates the resistance of the RC beam because of neglecting the membrane effect, where only 0.4MPa resistance load is predicted in comparison to over 0.75MPa load measured on the tested RC element. To propose a simplified improvement strategy, the UFC resistance function is amplified by the ratio of peak/yielding load estimated from the theoretical prediction in this study, while the descending behaviour and the further tensile membrane effect are ignored, representing the elastic-perfectly-plastic resistance function as in UFC, but with the modified peak load. The resistance function of this simplified approach is also shown in the figure.

It is worth noting that the computed static resistance diagram needs be adjusted by considering the dynamic increase factor (DIF) for steel and concrete to account for strain rate effect on the beam resistance capacity to blast load. Based on the measured strain rates and the design curves for DIFs provided in UFC [6], the averaged DIFs for concrete and steel of 1.30 and 1.34 are used, respectively in this study.

3.2.3. Comparison of the dynamic responses

Fig. 8 shows the comparison of the dynamic responses between Keenan's test results and the SDOF analysis results. A total of 6 groups of results are compared where specimen D1, D2 and D3 were subjected to low to high levels of blast loads. For instance, D1-6 stands for slab D1 in test number 6. The measured blast loads in Keenan's tests are simplified into equivalent triangular loads defined by the peak reflected pressures and the loading durations. Table 1 summarizes the loads, the maximum mid-span deflection, and the

corresponding time to the maximum deflections from both the tests and the analysis using different models. It should be noted that the maximum midspan deflection of test results of slab D1-7, D2-1, D2-2, D3-1 and D3-2 are not the data recorded by the displacement gage placed at midspan, but the recorded displacement at one thirds of the slab multiplied by 1.5. This is because according to Keenan, when the slab was under large inelastic deflections (greater than 30 mm), there occurred moderate to severe disintegration of concrete near midspan, the spalling concrete could have disturbed the mechanical connection between the deflection gage and slab thus causing inaccurate deflection measurements.

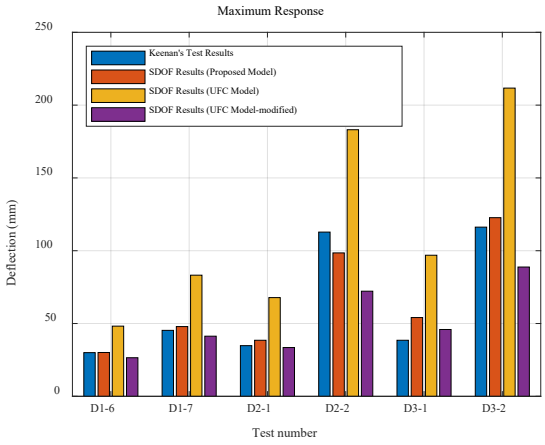

Fig. 8 Comparison of the maximum mid-span deflections

Table 1 Summary of dynamic test and SDOF analysis results

Slab No.	Equivalent load		Maximum mid-span deflection (mm)			
	P_r (kPa)	t_d (ms)	Test	Proposed model	UFC model	Modified UFC model
D1-6	931	11	30.0	30.1 (+0.3%)	38.5 (+28.3)	26.7 (-11.7%)
D1-7	1241	10	45.3*	47.9 (+5.7%)	77.1 (+70.2%)	41.9 (-8.8%)
D2-1	1069	11	34.8*	38.5 (+10.6%)	59.6 (+71.3%)	33.9 (-3.7%)
D2-2	1344	14	112.8*	98.5 (-12.7%)	181.9 (+61.3%)	73.6 (-36.0%)
D3-1	1269	10.6	38.5*	54.1 (+40.5%)	91.4 (+137.4%)	46.6 (+19.2%)
D3-2	1503	13	116.2*	122.7 (+5.6%)	213.7 (+83.9%)	90.8 (-23.6%)

Note: * means computed values obtained by multiplying the recorded displacement at one thirds of the slab by 1.5.

364 It can be observed from Fig. 8 and Table 1 that the maximum deflections of the slabs could be accurately
365 predicted by using the proposed model under both low and high intensity blast loadings with errors within
366 15%. As expected, using the UFC suggested model could significantly overestimate the maximum deflections
367 especially when the blast load is large and inelastic deformation becomes dominant. This is because the
368 contribution of the membrane effect to the resistance of the slab is neglected in the UFC method. It is also
369 noticed that when subjected to low-intensity blast loading for D1-6, D1-7, D2-1 and D3-1 where relatively
370 small mid-span deflection is resulted, the modified UFC model with the amplified resistance function by
371 considering the compressive membrane effect could provide relatively close predictions to those from the
372 proposed model and the testing results. However, when the deformation is large (D2-2 and D3-2), the
373 modified UFC model would still largely underestimate the maximum deflections. This is because at large
374 deflection, the descending of slab resistance and tensile membrane effect would strongly influence the
375 response of the slabs, and the modified UFC model could not capture these membrane effects.
376

377 ## 4. Parametric Studies

378 Parametric study is performed using the proposed model to examine the influences of design parameters on
379 the membrane effects. Without losing generality, the slab parameters (No. 4) in Woodson's test as described
380 above is taken as the default reference RC component here. The slabs' dimension is 609.6mm (clear span)×
381 609.6mm (width)×76.2mm (depth) The lateral stiffness at support, reinforcement ratio, and span to depth
382 ratio are varied to study their respective influences on the membrane effect of the RC element.

4.1. Influence of support lateral stiffness

To study the influence of support lateral stiffness on the membrane effect, the lateral stiffness at support, S_n is varied with the ratio of S_n / S_a (S_a is the axial stiffness of the slab) ranging between 0.005 to 10.

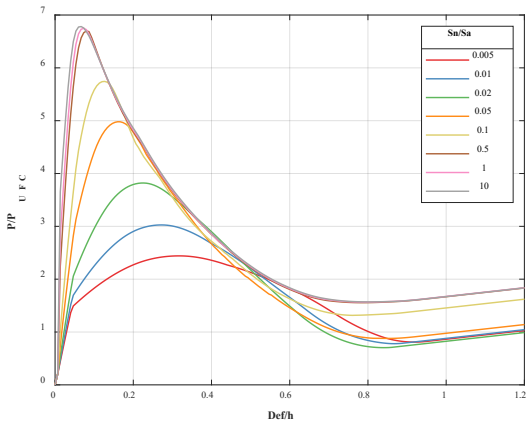

Fig. 9 Effects of lateral stiffness on load-deflection relationship of slab No. 4.

The resistance curves (resistance load versus mid-span deflection) are calculated using the proposed model. To better demonstrate the membrane effect, the resistance load P is normalized by the ultimate resistance calculated following UFC 3-340-02, P_{UFC}, where no membrane effect is considered. The mid-span deflection, *Def*, is also normalized against the depth of the slab h. As shown in Fig. 9, it is evident that the effect of the stiffness of the lateral restraint is significant on both the maximum resistance load and the shape of the load-deflection relationship. As the support goes stiffer, the maximum resistance load in the compressive membrane domain increases quicker, and the corresponding central deflection also reduces. When the support is flexible, the maximum resistance load reduces, which nevertheless is still larger than the UFC's resistance load (P/P_{UFC} is always larger than 1.0). When $S_n / S_a = 0.5$, very significant membrane action can be achieved. However, beyond this limit, further increase in support lateral stiffness would not significantly increase the compressive membrane action. It indicates that in engineering practice, to improve the resistance capacity of a RC element through introducing membrane effect, it is not necessary to create an

400 infinitely rigid support. In addition, it can be observed from Fig. 9 that the transition point from the
401 compressive membrane domain to the tensile membrane domain shifts from 0.76 to 0.87 for (*Def/h* ratio) as
402 the S_n/S_a ratio decreases from 10 to 0.005. This indicates that the transition point from the compressive
403 membrane domain to the tensile membrane domain occur later at a larger deflection when the support is more
404 flexible.

405 **4.2. Influence of reinforcement ratio**

406 To investigate the influence of reinforcement ratio on membrane effect, the resistance curves of the above
407 reference slab with varying reinforcement ratio from 0.25% to 2% is modeled. Fig. 10 shows the normalized
408 resistance load versus the central deflection over slab depth relationship. The lateral stiffness of support S_n
409 equals to S_a. It can be seen that as the reinforcement ratio increases, the enhancement of resistance capacity
410 induced by membrane effect decreases. For instance, with 0.25% reinforcement, considering the membrane
411 effects leads to an increase of 6.7 times of the peak resistance load P/P_{UFC}, which quickly reduces to only 1.7
412 times when reinforcement ratio is 2%. This is because with a high reinforcement ratio, the axial elongation of
413 the slab would be effectively restrained by the reinforcement. Therefore, less movement at the support to
414 induce the compressive membrane force. However, the corresponding deflection at the maximum resistance
415 load appears to be unaffected by the reinforcement ratio. Similar phenomenon was also observed in
416 Woodson's test [12]. Besides, as the reinforcement ratio increases, the load and deflection of the transition
417 point would both slightly decrease and eventually approach to the tensile membrane line initiated from the
418 origin. This might be because concrete in compression region is more prone to crush when reinforcement ratio
419 is higher, which would lead to the descending branch of compressive membrane curve (segment AB in Fig. 5)

to intersect with the pure tensile membrane line.

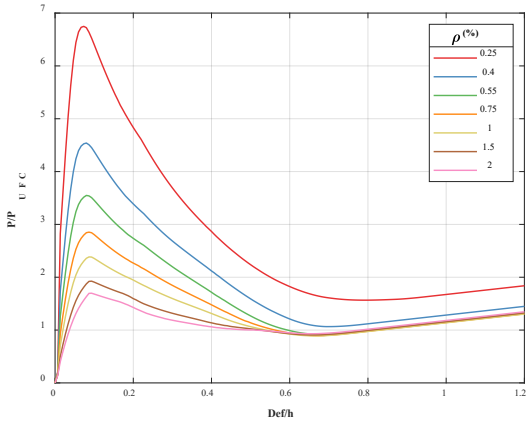

Fig. 10 Effects of reinforcement ratio on load-deflection relationship of slab No. 4.

4.3. Influence of span-to-depth ratio

To study the influence of the span-to-depth ratio on the resistance curve, the ratio of clear span over slab depth is varied between 8 and 30 by changing the value of clear span, where the other parameters for the reference slab is maintained as constant. As shown in Fig. 11, more pronounced enhancement on loading resistance from the membrane action can be found on the slab with a smaller span-to-depth ratio, resulting in a larger resistance load and a larger initial stiffness. For example, when L/h=8, the peak resistance load ratio is 6.7 at Def/h=0.073; when L/h=30, the peak load ratio is 2.0 at Def/h=0.31. This is because the moment of inertia of a deep beam is larger than that of a shallow beam. Therefore, a deep beam has a larger stiffness in the compressive membrane domain of the resistance function. Under the same level of rotation at the beam ends, a larger compressive membrane force is therefore induced in a deep beam than in a shallow beam. The same observation was also reported by Woodson in his laboratory test [21] that the peak loading capacity in deep slabs was increased more at much smaller Def/h values than those in slender slabs. The results also show that the transition point is less sensitive to the span to depth ratio.

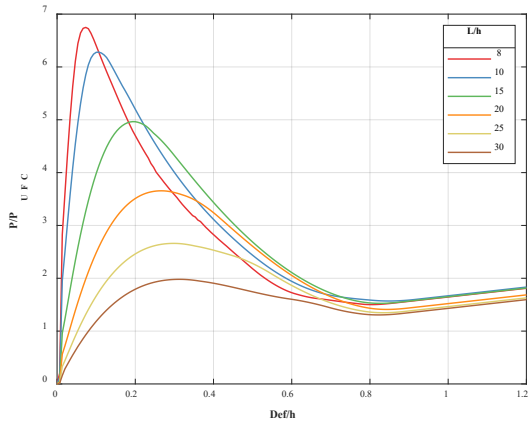

Fig. 11 Effects of span-to-depth ratio on load-deflection relationship of slab No. 4.

4.4. Summary

Based on the parametric studies described above, it can be concluded that the membrane actions can be significantly affected by the lateral stiffness of support, reinforcement ratio and span-to-depth ratio. Generally, stiff boundary conditions, low reinforcement ratio and small span correspond to the more significant contributions to load resistance from the membrane effects.

Usually, when the stiffness of the support and the structural element are in similar level, significant increment of load-carrying capacity can be obtained due to compressive membrane effect. Further increasing the stiffness of the support would not significantly improve the load-resistance capacity of the structural element. Membrane effect is more pronounced to a less reinforced structural element than a heavily reinforcement element because the normal loading-resistance capacity of a less reinforcement element is small. Besides, properly anchoring the reinforcements leads to more reserve capacity of the elements with high reinforcement ratio. A thicker RC element could achieve more pronounced membrane effect than a thinner one with the same span. Nevertheless, the thicker element could be more prone to shear failure, which leads to a reduced load-carrying capacity. Therefore, those parameters need to be properly balanced in the design.

5. Modification coefficient diagrams

The above results demonstrate that considering the membrane effect leads to more accurate predictions of the loading capacity of reinforced concrete beams to resist blast loads than the UFC approach without considering the membrane effect. In this section, loading capacities of RC beams of different configurations are calculated using the proposed approach in this study for better estimation of RC beam blast loading resistance capacities. The results are presented as modification coefficients of the loading capacity calculated using the UFC approach without considering the membrane effects, i.e., P_m/P_{UFC}, in which P_m is the loading capacity obtained with consideration of the membrane effect, and P_{UFC} is the loading capacity obtained from UFC design guides based on elastic-perfect-plastic resistance assumption. In design analysis, the loading capacity can be estimated from UFC design charts first, if more accurate loading capacity prediction is needed, the UFC based loading capacity can be corrected by using the modification coefficient derived in this study. Based on the parametric studies described above, the lateral stiffness of the support, reinforcement ratio and span-to-depth ratio significantly affect the contributions of membrane effects on loading capacities of RC beams. Therefore, the modification coefficients are derived with respect to these three parameters. For easy application, the modification coefficients are presented in diagram form by plotting the modification coefficient as a function of the stiffness ratio (S_n/S_a) and reinforcement ratio (r_o) for different span to depth ratios *(L/h)*. It should be noted that the rotational stiffness (S_m) is assumed as infinity in these analyses.

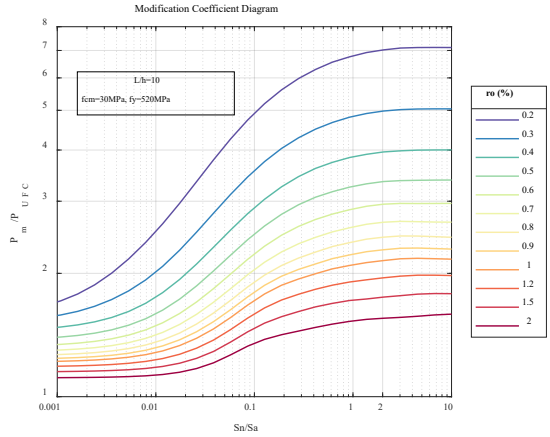
Modification Coefficient Diagram
L/h=10
fcm=30MPa, fy=520MPa
P m /P U F C
Sn/Sa
ro (%)
0.2
0.3
0.4
0.5
0.6
0.7
0.8
0.9
1
1.2
1.5
2

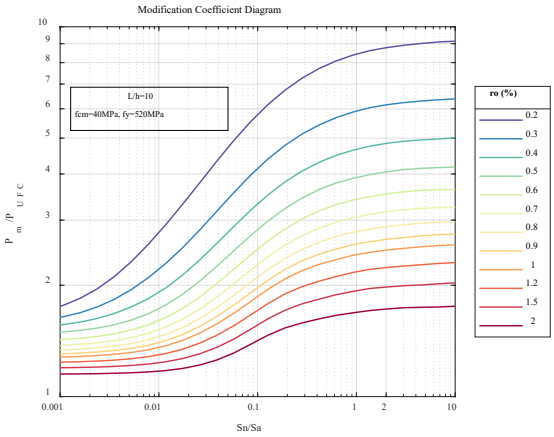
Modification Coefficient Diagram
L/h=10
fcm=40MPa, fy=520MPa
P m /P U F C
Sn/Sa
ro (%)
0.2
0.3
0.4
0.5
0.6
0.7
0.8
0.9
1
1.2
1.5
2

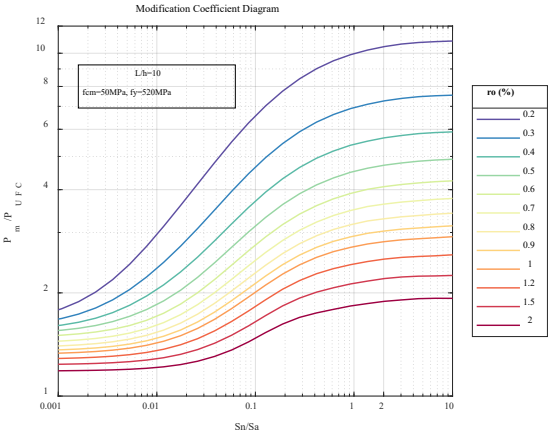
Modification Coefficient Diagram
L/h=10
fcm=50MPa, fy=520MPa
P m /P U F C
Sn/Sa
ro (%)
0.2
0.3
0.4
0.5
0.6
0.7
0.8
0.9
1
1.2
1.5
2

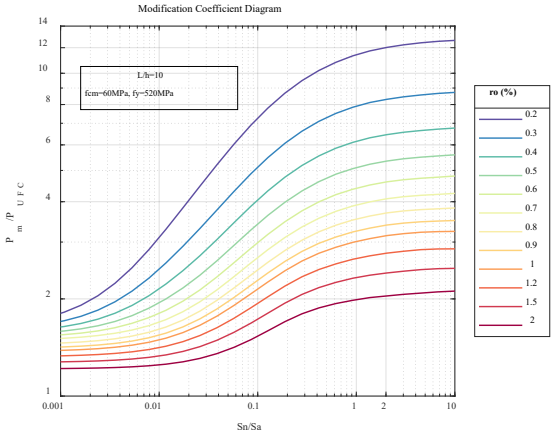
Modification Coefficient Diagram
L/h=10
fcm=60MPa, fy=520MPa
P m /P U F C
Sn/Sa
ro (%)
0.2
0.3
0.4
0.5
0.6
0.7
0.8
0.9
1
1.2
1.5
2

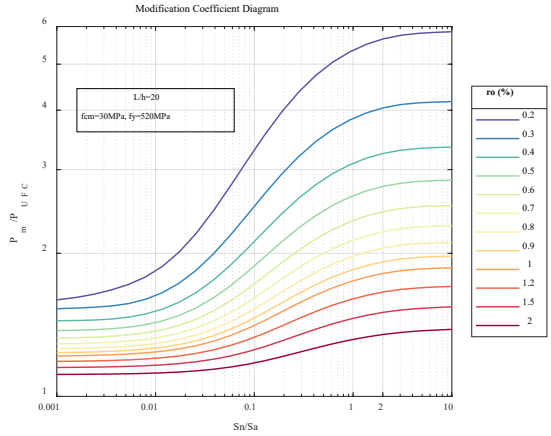
Modification Coefficient Diagram
L/h=20
fcm=30MPa, fy=520MPa
P m /P U F C
Sn/Sa
ro (%)
0.2
0.3
0.4
0.5
0.6
0.7
0.8
0.9
1
1.2
1.5
2

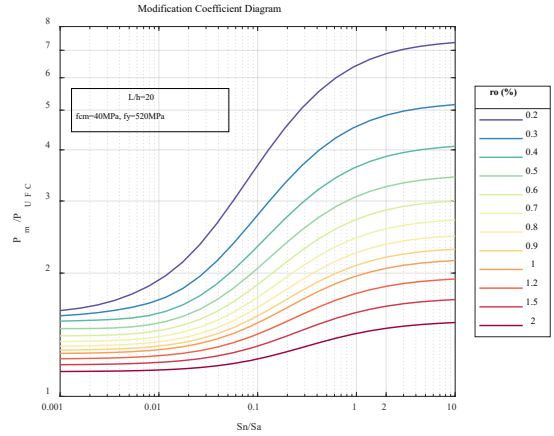
Modification Coefficient Diagram
L/h=20
fcm=40MPa, fy=520MPa
P m /P U F C
Sn/Sa
ro (%)
0.2
0.3
0.4
0.5
0.6
0.7
0.8
0.9
1
1.2
1.5
2

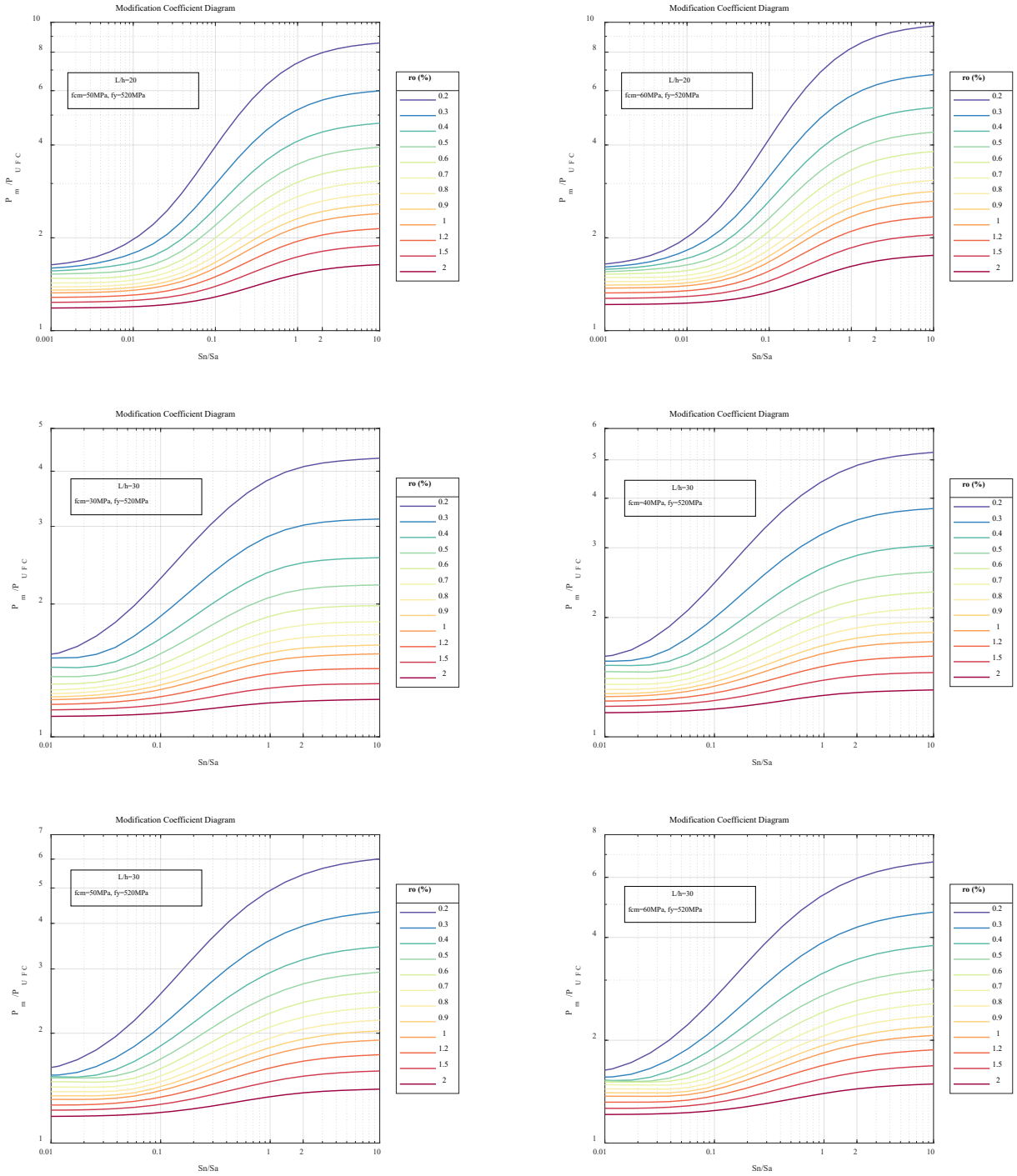

469 Fig. 12 Modification coefficient diagrams for predicting the loading capacities with consideration of

470 membrane effect of restrained RC beams subjected to distributed load.

471 Fig. 12 gives the derived modification coefficient diagrams for RC beams of different configurations

472 corresponding to the design values given in UFC 3-340-02. Because of the large range of variables, the

473 logarithmic coordinates are used. Among these diagrams, three levels of span-to-depth ratio (L/h=10, 20, 30)

474 and four grades of concrete strength (f_{cm}=30, 40, 50, 60 MPa) are defined which cover the common designing
475 parameters of structural RC elements. Reinforcement strength also affects the membrane effects, but its
476 influence is actually equivalent to that caused by the reinforcement ratio. Therefore, if the reinforcement
477 strength is different from 520 MPa, its influence can be equivalently accounted for by adjusting the
478 reinforcement ratio. Interpolation method can be used to approximately obtain the modification coefficient
479 with other designing parameters.

480 From Fig. 12 it can be observed that all these coefficient curves are "S" shaped. When the stiffness ratio
481 is small, the modification coefficient increases slowly; as the stiffness ratio increases, the modification
482 coefficient increases more rapidly, and then the rate of increment becomes slow again when the stiffness ratio
483 is large, and the growth rate declines gradually to zero with the stiffness ratio. It may be noticed that when the
484 stiffness ratio approaches zero, the modification coefficient does not approach to unity. This is because the
485 rotational stiffness is assumed to be infinity which also increases the resistance. As discussed in the parametric
486 studies, the enhancement on the loading resistance capacity from the membrane effect decreases as
487 reinforcement ratio or span-to-depth ratio increases. Besides, as concrete strength increases, modification
488 coefficient would also increase, which is expected since concrete with a higher strength could bear a higher
489 compressive membrane force which leads to a higher enhancement on the resistance capacity.

490 6. Conclusion

491 In this paper, an analytical model considering both the compressive and tensile membrane actions is
492 proposed to depict the resistance function of RC element subjected to uniformly distributed load. A complete
493 load-deflection curve is derived, which can be used in dynamic analysis of structural elements under blast
494 loads. Compared to the previous model and existing design method, the proposed model considers both the

concrete strength degradation caused by concrete crushing and the reserve capacity induced by tensile membrane action, therefore could provide a more accurate load-deflection curve. The proposed model is validated with existing laboratory static and field blast test results. It is found that the proposed model could closely depict the resistance function and therefore leads to more accurate predictions of the dynamic response of RC elements subjected to blast loads.

Parametric study is carried out to investigate the influence of lateral stiffness of support, reinforcement ratio and the span-to-depth ratio on the membrane effect. It is found that a stiff boundary, low reinforcement ratio and small span to depth ratio increase the membrane effect on loading resistance capacities of RC members.

For easy engineering applications, a series of modification coefficient diagrams are generated using the proposed model to correct the predicted loading capacities from UFC charts without considering the membrane effects. These modification coefficients can be used together with UFC design charts to quickly and more accurately predict the structural capacities to resist blast loads.

Acknowledgement

The first three authors would like to acknowledge the financial support from Australian Research Council under ARC-Discovery Project fund DP190103253.

Reference

[1] Wikipedia (2020). "2020 Beirut explosion." <https://en.wikipedia.org/wiki/2020_Beirut_explosion>. (18 July, 2021).

[2] Burrell RP, Aoude H, Saatcioglu M. Response of SFRC Columns under Blast Loads. Journal of Structural Engineering. 2014;141:04014209.

[3] Shi Y, Hao H, Li Z-X. Numerical derivation of pressure–impulse diagrams for prediction of RC column damage to blast loads. International Journal of Impact Engineering. 2008;35:1213-27.

[4] Carta G, Stochino F. Theoretical models to predict the flexural failure of reinforced concrete beams under blast loads. Engineering Structures. 2013;49:306-15.

[5] Desayi P, Kulkarni AB. Load-deflection behavior of restrained RC slabs. Journal of the Structural Division. 1977;103:405-19.

[6] UFC3-340-02. Structures to resist the effects of accidental explosions. Washington DC, Unified Facilities Criteria. 2008.

[7] Keenan WA. STRENGTH AND BEHAVIOR OF LACED REINFORCED CONCRETE SLABS UNDER STATIC DYNAMIC LOAD. NAVAL CIVIL ENGINEERING LAB PORT HUENEME CALIF; 1969.

[8] Keenan WA. Strength and behavior of restrained reinforced concrete slabs under static and dynamic loadings. NAVAL CIVIL ENGINEERING LAB PORT HUENEME CA; 1969.

[9] Christiansen KP. The effect of membrane stresses on the ultimate strength of the interior panel in a reinforced concrete slab. The Structural Engineer. 1963;41:261-5.

[10] Krauthammer T. Modern protective structures. Boca Raton: CRC Press; 2008.

[11] Park R, Gamble WL. Reinforced concrete slabs. New York: John Wiley & Sons; 2000.

[12] Woodson SC. Effects of shear reinforcement on the large-deflection behavior of reinforced concrete slabs. ARMY ENGINEER WATERWAYS EXPERIMENT STATION VICKSBURG MS STRUCTURES LAB; 1994.

[13] Qian Q, Wang M. Calculation theory for advanced protective structure. Nanjing: Phoenix Publishing. 2009.

[14] Chen L, Fang Q, Guo Z, Liu J. An improved analytical method for restrained RC structures subjected to static and dynamic loads. International Journal of Structural Stability and Dynamics. 2014;14:1350052.

536 [15] Park R. Tensile membrane behaviour of uniformly loaded rectangular reinforced concrete slabs with fully restrained
537 edges. Magazine of Concrete Research. 1964;16:39-44.
538 [16] Astarlioglu S, Krauthammer T, Morency D, Tran TP. Behavior of reinforced concrete columns under combined
539 effects of axial and blast-induced transverse loads. Engineering Structures. 2013;55:26-34
540 [17] Krauthammer T. Shallow-Buried RC Box-Type Structures. Journal of Structural Engineering. 1984;110:637-51.
541 [18] Hognestad E. Study of combined bending and axial load in reinforced concrete members. University of Illinois at
542 Urbana Champaign, College of Engineering, Experiment Station. 1951.
543 [19] Biggs JM. Introduction to structural dynamics. New York: McGraw-Hill Book Company; 1964.
544 [20] Fujikake K, Li B, Soeun S. Impact Response of Reinforced Concrete Beam and Its Analytical Evaluation. Journal of
545 Structural Engineering. 2009;135:938-50.
546 [21] Woodson SC. Shear Reinforcement in Deep Slabs. ARMY ENGINEER WATERWAYS EXPERIMENT STATION
547 VICKSBURG MS STRUCTURES LAB; 1994.
548